Materials Today Physics 29 (2022) 100906

Contents lists available at ScienceDirect

Materials Today Physics

journal homepage: www.journals.elsevier.com/materials-today-physics

Characterizations on the doping of single-crystal silicon carbide

Huifan Xiong [a,b], Weiwei Mao [c], Rong Wang [a,b], Shuai Liu [a,b], Naifu Zhang [b], Lihui Song [a,b,*], Deren Yang [a,b], Xiaodong Pi [a,b,**]

[a] State Key Laboratory of Silicon Materials & School of Materials Science and Engineering, Zhejiang University, Hangzhou 310027, China
[b] Institute of Advanced Semiconductors & Zhejiang Provincial Key Laboratory of Power Semiconductor Materials and Devices, ZJU-Hangzhou Global Scientific and Technological Innovation Center, Zhejiang University, Hangzhou 311200, China
[c] Key Laboratory of Optical Field Manipulation of Zhejiang Province & Department of Physics, Zhejiang Sci-Tech University, Hangzhou 310018, China

ARTICLE INFO

Keywords:
Silicon carbide doping
Elemental analysis
Optical characterization
Electrical characterization

ABSTRACT

Due to its intriguingly electrical, thermal and optical characteristics, single-crystal silicon carbide (SiC), one of the most significant wide-bandgap semiconductors, has been receiving intense attention. Up to date, SiC has been investigated for applications in high-power and high-frequency electronics, ultraviolet optoelectronics and quantum computing, which all critically have a strict requirement on the doping of SiC. To improve the quality and reliability of SiC devices, the amounts of both intentionally and unintentionally doped impurities as well as the doping-dependent characteristics like resistivity must be characterized with accuracy and convenience. This article reviews these characterization methods, including elemental analysis, electrical and optical methods. Among those, the term "elemental analysis" dominantly introduces the secondary ion mass spectroscopy technique (SIMS). Meanwhile, for the electrical methods, we will discuss the mature techniques used in laboratory including the Hall effect method, the electrical scanning probe techniques, etc. Moreover, the optical methods introduce the optical absorption method, Raman spectra analysis and photoluminescence spectroscopy. Additionally, a focus is placed specifically on the characterization of the carrier concentration distribution in SiC wafer, which meets the practical requirement for in situ diagnostics of SiC wafers.

1. Introduction

Single-crystal silicon carbide (SiC) inherits the remarkable properties of wide bandgap semiconductor, such as high thermal conductivity, high breakdown field and high saturation velocity. SiC has a variety of excellent properties with the different polytypes (Tab. 1), and therefore provides benefits in devices operating at high frequency, high power, high temperature, as well as in a harsh environment. Furthermore, SiC has been used in a variety of useful devices including High-Electron Mobility Transistor (HEMT) [1], Metal-Oxide Field Effect Transistors (MOSFETs) [2], Insulated Gate Bipolar Transistor (IGBT) [3] and Junction Field-Effect Transistor (JFET) [4]. Moreover, SiC is used for manufacturing integrated circuits and inverters, with the development, it has been applied in the civil field such as powertrain of electric vehicles [5,6]. In addition, utilizing certain defects in SiC have emerged as a promising platform for quantum communication [7,8]. It is worth noting that the formation of these defects depends on dopants. For example, the dopants are of importance for the stability and charge states of these defects and may lead to the formation of dopant-related vacancy-complexes [9,10]. In order to manufacture these devices and products, accurately controlling dopant and impurity levels of n-type, p-type and semi-insulation of SiC are essential.

Physical vapor transport (PVT), also known as the Modified Lely method, is a common technique for preparing single-crystal SiC [14,15]. To obtain n-type SiC [16], nitrogen (N) or phosphorus (P) is usually doped. Additionally, aluminum (Al) or boron (B) is generally doped to obtain p-type SiC [17,18], and vanadium (V) is doped to obtain semi-insulating SiC [11,19,20]. Background impurities comprising different metallic impurities like Al, Ti, B, Fe [21] and non-metallic impurities such as N, P, S always have an adverse effect on the formation of SiC single crystals. Tab. 2 displays the background impurity concentration in one certain SiC powder source and the nominally undoped as-grown SiC sample for reference. In general, a low and controlled electrically active impurities background is required for the

* Corresponding author. State Key Laboratory of Silicon Materials & School of Materials Science and Engineering, Zhejiang University, Hangzhou 310027, China.
** Corresponding author. State Key Laboratory of Silicon Materials & School of Materials Science and Engineering, Zhejiang University, Hangzhou 310027, China.
E-mail addresses: songlihui@zju.edu.cn (L. Song), xdpi@zju.edu.cn (X. Pi).

https://doi.org/10.1016/j.mtphys.2022.100906
Received 19 September 2022; Received in revised form 26 October 2022; Accepted 1 November 2022
Available online 2 November 2022

Table 1
Some critical properties of 4H–SiC, 6H–SiC, 3C–SiC and Si [11,12].

	4H–SiC	6H–SiC	3C–SiC	Si
Bandgap (eV)	3.26	3.02	2.39	1.11
Breakdown field (10 [6] V/cm)	~3	~3	~4	~0.25
Thermal conductivity (W/cm/K)	4.9	4.9	5	1.5
Electron saturated drift velocity (10 [7] cm/s)	2.2	1.9	2	1

Table 2
Chemical analysis (GDMS) of impurities in SiC powder (source) and a nominally undoped as-grown SiC sample [13].

Units (ppm wt)	N	P	S	B	Al	V	Cu	Ni
Source	<500	0.17	1.5	0.28	0.5	0.02	2.0	0.62
Crystal	6	0.03	0.11	0.08	0.02	<0.005	0.1	0.04

reproducible growth of semi-insulation SiC wafers and lowly doped SiC epi-layers, so it is important to accurately characterize the diverse electrically active impurities which can introduce donor or acceptor energy levels [22]. Moreover, knowing how many impurities have been incorporated into SiC is a prerequisite for achieving a specific doping concentration. As a result, to obtain approved SiC wafers, accurate and practical inspection technologies are necessary, which can provide advantages for mass manufacture of high-quality SiC devices.

It is crucial to precisely determine the concentrations of impurities doped in SiC intentionally and unintentionally. One of the elemental analysis techniques, secondary ion mass spectroscopy (SIMS), is a strong contender to determine the concentrations of all impurities in SiC with excellent resolution and a low detection limit. However, SIMS is a micro-area analysis method that only measures the chemically incorporated impurity concentration and is rarely used to measure over the whole wafer with a larger area. It is also unable to distinguish whether the measured impurities are electrically active or not in SiC wafer. Most of the time, it is preferable to measure electrical characteristics such as carrier concentration and resistivity that are associated with the impurities incorporated into SiC wafer, since electrical characteristics directly show the interaction results of all active impurities in SiC wafer. Therefore, electrical methods including the Hall effect measurement method for measuring average carrier concentration and resistivity, and contactless resistivity mapper techniques for measuring the spatial distribution of resistivity are comprehensively discussed in this paper. Nevertheless, it is worth noting that the parameters derived by the conventional electrical methods are average values for the entire area detected and therefore the resolution is low. Hence, a precise measurement method is essential that is able to measure the characteristics of every micro-region of SiC wafers. Electrical scanning probe techniques have been explored to measure the lateral and cross-sectional distribution of electrical characteristics of SiC materials and subsequent devices in nanoscale. However, to guarantee high resolution, the electrical scanning probe techniques could only detect small region and therefore is not suitable for wafer-scale measuring. Fortunately, some certain optical methods can make up for this shortcoming. The optical methods, as the representative contactless measuring methods, are generally used to characterize the spatial distribution and even depth profile of carrier concentration in SiC within a much larger region with a resolution of micrometers. In this paper, the optical methods including optical absorption method, Raman spectra analysis, and photoluminescence spectroscopy are discussed, which are practical for process monitoring due to their less time consuming. However, prior to use for quantitative determination, the data from the optical methods must be calibrated with some electrical methods. Overall, this paper will provide a thorough review and comparison of elemental analysis, electrical and optical methods (Fig. 1).

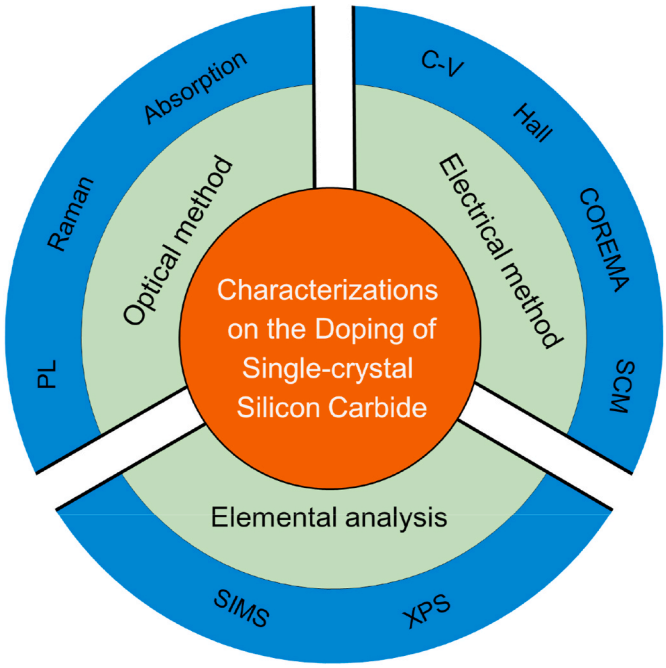

Fig. 1. Skeleton diagram of common characterization methods for the doping of single-crystal SiC.

Virtually all of the existing research literature has focused on a particular characterization technique for single-crystal SiC, but none of the updated review publications has so far summarized the pertinent problems. This review aims to provide a concise summary of popular characterization methods regarding SiC doping. In section 2, elemental analysis techniques sensitive to the whole impurities existing in single-crystal SiC are covered in detail. The electrical methods are then provided and contrasted in section 3 in terms of measuring the resistivity and carrier concentration of SiC. Additionally, section 4 discusses the optical methods for determining the spatial distribution of carrier concentration. Finally in section 5, some observations and conclusions are offered together with predictions for the future of this topic.

2. Elemental analysis

Through component analysis, it is possible to directly characterize the concentration of genuine doped elements, among which secondary ion mass spectroscopy (SIMS) is one representative test method for material surface composition analysis [23]. SIMS can be broadly divided into Dynamic Secondary Ion Mass Spectrometry (D-SIMS) and Time-of-Flight Secondary Ion Mass Spectrometry (ToF-SIMS). Sputtering rate and ion yield are the main differences between D-SIMS with a higher primary ion current and ToF-SIMS which is referred to as “static” SIMS with a low primary ion current [24]. In addition, X-ray photoelectron spectroscopy (XPS), among other elemental analysis methods, is one of the semi-quantitative elemental analysis tools with a fairly lower sensitivity than SIMS that can reveal chemical bond information [25,26]. This section focuses on SIMS since it is frequently used to characterize the impurities in SiC due to its high mass resolution and high sensitivity to trace elements or compounds.

2.1. Fundamental principle and applications of SIMS

SIMS instruments use an internally generated beam of either positive or negative ions (primary ion current) focused on a sample surface to generate single ions and molecules with electric charges (secondary ions) that are then separated by a high electrostatic potential and detected by a mass analyzer (Fig. 2b). Despite being a semi-quantitative

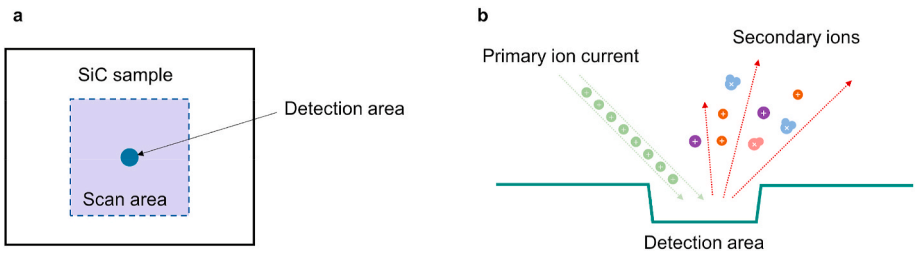

Fig. 2. Schematic diagram of the SIMS technique. a, Detection area (green) and scan area (purple) in SiC sample characterized by SIMS. **b,** Primary ion current bombard the SiC surface liberating single ions and molecular compounds.

analysis method, SIMS can nevertheless be used to measure the impurities concentration with a detection limit of ppm level and even ppb level. It can examine a sample to a depth of several atomic layers within 1–10 nm that can be used to measure surface contamination. Furthermore, the SIMS technique has a high spatial resolution which is determined by the spot size of the primary ion current. In detail, a focused primary ion current has a spot size between 1 μm and 20 μm, and utilizing the scan mode, all the pixels split from the scan area can be used to create an image of impurity concentration distribution on the sample surface (Fig. 2a).

The distribution of various impurities along the depth direction can be obtained in depth profiling mode, which is one of the classic and usual techniques of SIMS used in SiC and especially in ions implantation profiles and the interface of SiO_2/SiC [27–29]. In order to inject specified electrical dopants into SiC in the device manufacturing process, ion implantation is indispensable, which embodies the importance of the depth profiling technique of SIMS [30]. High resolution is necessary for SIMS, because as a result of ion mixing and knock-on effect, artifact depth profiles will be shown with a broadening in depth. In recent years, the resolution of depth profiling has been developed to sub-nm by using dual-beam ToF-SIMS, which can suppress ion mixing and knock-on effect [31]. Additionally, the scan mode can be used with the depth profile analysis approach to capture spectral images of every pixel in the scan area at every depth. Fig. 3a displays the depth distribution of three species using the depth profile analysis method, and the spectral images (summed over all depths) of the scan area are shown in Fig. 3b [32]. Additionally, three-dimensional (3D) images of surface and internal chemical components can be obtained with the help of sample

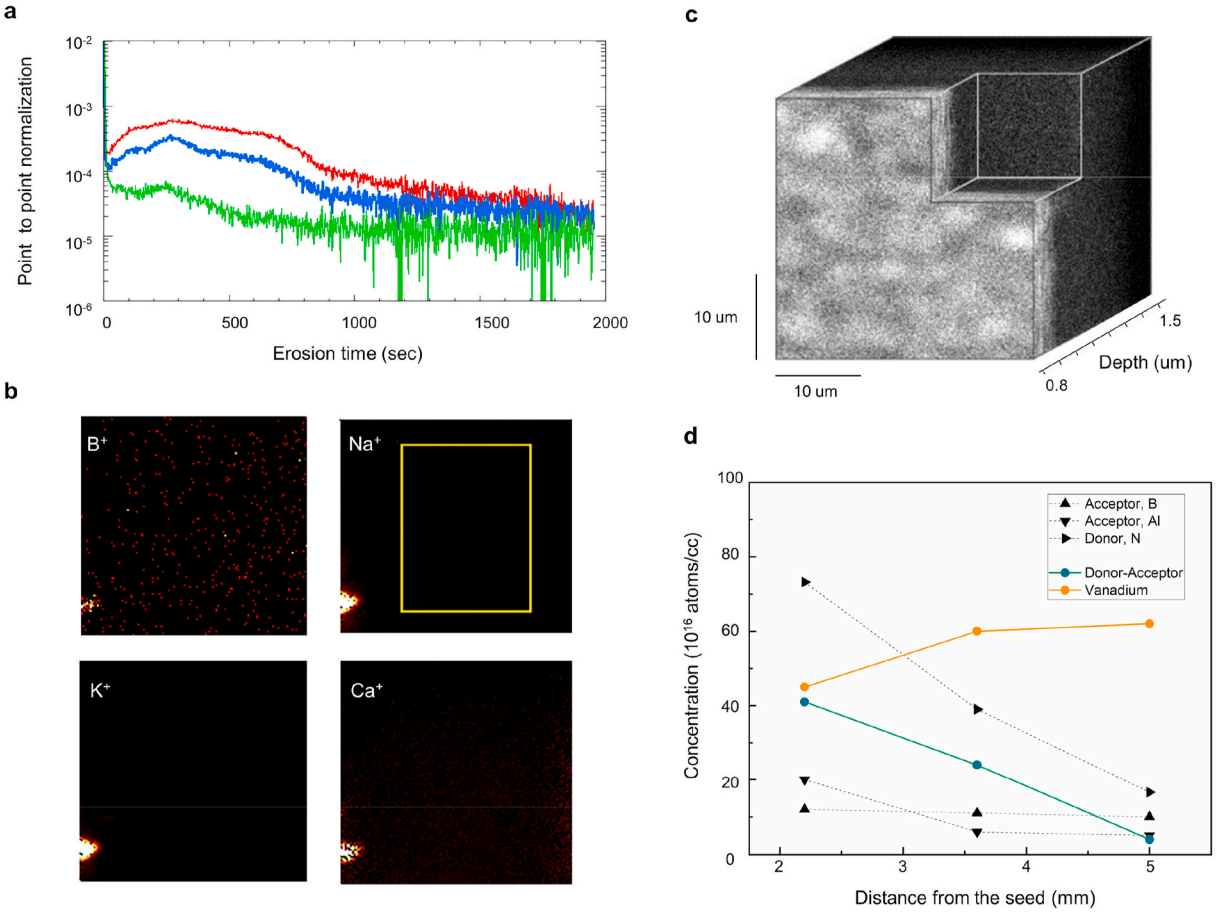

Fig. 3. | The impurities distribution in SiC measured from SIMS. a, Depth distribution of three species [Na^+ (red), K^+ (blue), and Ca^+ (green)] which were not expected to be in SiC. **b**, Spectral images of B^+, Na^+, K^+, and Ca^+ (summed over all depths) constructed from the depth profile shown in **a.** The scan area is 200 × 200 μm^2 with a pixel density of 128 × 128. Reproduced from Ref. [32], copyright 2021, AIP Publishing LLC. **c**, 3D SIMS image of the ^{11}B concentration for a 4H–SiC sample (the brighter region represents higher boron concentration). Reproduced from Ref. [33], copyright 2006, Elsevier B.V. **d**, Impurity analysis of V-doped SiC ingot using dynamic SIMS along growing direction. Reproduced from Ref. [34], copyright 2018, Elsevier B.V.

surface scanning and depth profiling. Fig. 3c shows a 3D image of the distribution of boron doping concentration, where the brighter region represents higher boron concentration [33]. Even though the 3D image has a high resolution, only a very tiny bulk of SiC can be displayed. Whereas for large bulk SiC on the size of centimeter or above, it is a good choice to measure several areas along the same direction selected by SIMS. For instance, divide the SiC ingots into multiple wafers and use SIMS to measure the concentration of the impurities in the selected areas of the wafers. Fig. 3d shows the impurity distribution measured by SIMS along the growing direction in a vanadium-doped SiC ingot [34], where the donor-acceptor is the difference between the donor impurities concentration and acceptor impurities concentration.

2.2. Challenge and the solution

SIMS can be used to identify several electrical dopants in SiC such as N, P, Al, B and V as well as some background impurities such as O, Ti, Ni, and Cu. The impurities in SiC crystals are more detrimental to semi-insulating and light doping single-crystal SiC. Therefore, it is crucial to have a precise measuring technique with a low enough detection limit to quantify the influential impurities such as N. Tab. 3 shows the detection limits of the main elements in SiC by SIMS [35]. Generally, a faster sputter rate with high ion yield will produce high ionization efficiency and greater detection limits, but result in worse depth resolution and fewer data points. Furthermore, it is necessary to select appropriate primary ion beam current to control sputter rate. To improve the detection limits of the impurities by SIMS, raster change technique is developed [36], which alters the size of the primary ions beam during a profile at the same position on the SiC sample. Raster change technique has been reported to obtain a low detection limit for N in single-crystal SiC [37].

SIMS also has evident shortcomings. SIMS is a destructive and time-consuming measurement method with expensive and cumbersome equipment, that has no experimental repeatability. Only the chemically incorporated concentration of the element can be determined by SIMS, whereas other information like ionized impurity concentration or carrier concentration can not be determined, which is the key parameter for SiC wafer. Other methods must be combined with SIMS to characterize the doping of SiC, otherwise it is difficult to directly obtain the electrical parameters of SiC wafer.

3. Electrical methods

The electrical properties of SiC wafers related to their doping directly determine whether or not their quality meets the requirements for manufacturing qualified devices. Meanwhile, appropriate characterization techniques are also required to ascertain whether the electrical characteristics of SiC wafers are qualified for practical applications. A precondition for enhancing the SiC material quality and device performance is the precise characterization of its electrical properties. Therefore, we write at great length here about the electrical characterization methods for measuring resistivity and carrier concentration of SiC wafer. The conventional techniques such as Hall effect method tend to be used to measure SiC wafers or simple devices. Whereas, the novel electrical scanning probe techniques have usually been applied to characterize SiC interfaces and the inner structure of various devices like the channel region in SiC super-junction.

Table 3
The detection limits of common elements in SiC under depth profile conditions [35].

Element	Primary beam	Monitored Ion	Detection limit (atoms/cm^3)
N	(10–14.5 keV) Cs^+	$(^{12}C^+{}^{14}N)^-$	2×10^{15}, 3×10^{14} (bulk)
P	(10–14.5 keV) Cs^+	$^{31}P^+$	2×10^{14}
Al	(3–8 keV) O_2^+	$^{27}Al^+$	2×10^{13}
B	(3–8 keV) O_2^+	$^{11}B^+$	2×10^{13}
O	(10–14.5 keV) Cs^+	$^{16}O^-$	5×10^{16}, 1×10^{16} (bulk)
Ni	(3–8 keV) O_2^+	$^{58}Ni^+$	3×10^{14}
Cu	(3–8 keV) O_2^+	$^{63}Cu^+/^{65}Cu^+$	2×10^{14}
Fe	(3–8 keV) O_2^+	$^{54}Fe^+/^{56}Fe^+$	5×10^{13}
Na	(3–8 keV) O_2^+	$^{23}Na^+$	2×10^{13}
K	(3–8 keV) O_2^+	$^{39}K^+$	5×10^{12}
Cr	(3–8 keV) O_2^+	$^{52}Cr^+$	5×10^{13}
Ti	(3–8 keV) O_2^+	$^{48}Ti^+(no^{48}Ca^+)/^{47}Ti^+(no^{48}Ca^+)$	5×10^{12}

3.1. Conventional techniques

3.1.1. Characterization of resistivity

The on-state resistance and hence the power loss of the devices are directly impacted by the resistivity of SiC. Therefore, reliable and practical techniques for the characterization of resistivity are crucial. The resistivity is influenced by both carrier concentration and carrier mobility, and for the typical type of SiC wafer the carrier concentration is the determinant factor of resistivity. Hence, the characterization of resistivity can reveal the doping level of SiC.

Resistance is the ratio of voltage to current, and the probe method is effective in obtaining voltage and current values. In operation, with a constant current flowing into several regions of the SiC wafer, a mapping of voltage can then be obtained, and subsequently the mapping of resistivity is extracted from the voltage mapping image [38]. Nevertheless, this method is seldom employed as it lacks the precision of characterization and sample preparation is complicated. The non-contact eddy current method is a feasible method to determine the resistivity of conductive SiC wafers. But it still has some shortcomings. For instance, the non-contact eddy current method can only provide the average resistivity throughout the entire wafer, which also needs to be calibrated with a standard sample. Except for the above methods, Hall effect can be used to determine the resistivity of SiC wafer using van der Pauw measurement method [39]. An extended function of van der Pauw method is measuring the variation of resistivity with temperature change. Fig. 4a depicts the resistivity variation of the bulk semi-insulating 4H–SiC sample during the cooling and heating process [40]. Additionally, a drifting of device reading due to the trap effect throughout the temperature increase cycle is present.

Resistivity mapping techniques are a more effective method to quantify the distribution of resistivity in SiC wafer. A powerful diagnostic tool to evaluate the resistivity of semi-insulating SiC with high precision and repeatability is the COREMA system, a representative of the contactless resistivity mapper technique. The COREMA system uses a capacitive detector to measure the charge dynamic distribution in SiC wafers to calculate the resistivity, and the measurement time is less than a minute, which takes significantly less time than that of traditional resistivity measurement methods. Fig. 4b shows a resistivity mapping of V-doped semi-insulating SiC wafer, where high resistivity parts are displayed as red regions. Similarly, n-type or p-type SiC wafer can as well be characterized using resistivity mapper techniques [41,42]. Fig. 4c and d, respectively, show a resistivity mapping of SiC doped with high aluminum content [43] and a resistivity mapping for an Al and B co-doped 4H–SiC wafer [44]. Besides, the histograms of the resistivity occupancy ratio for both cases are demonstrated on the right.

3.1.2. Characterization of carrier concentration

Carrier concentration and resistivity are related, but as the exact value of mobility is hard to determine, they are typically measured separately. Furthermore, the measurement of carrier concentration can be used to estimate the doping concentration if the SiC wafer is homogeneously doped and free of other impurities except for dopants. Otherwise, the concentrations of the carrier and doping can differ significantly for non-homogeneous doping. And additionally, for n-type

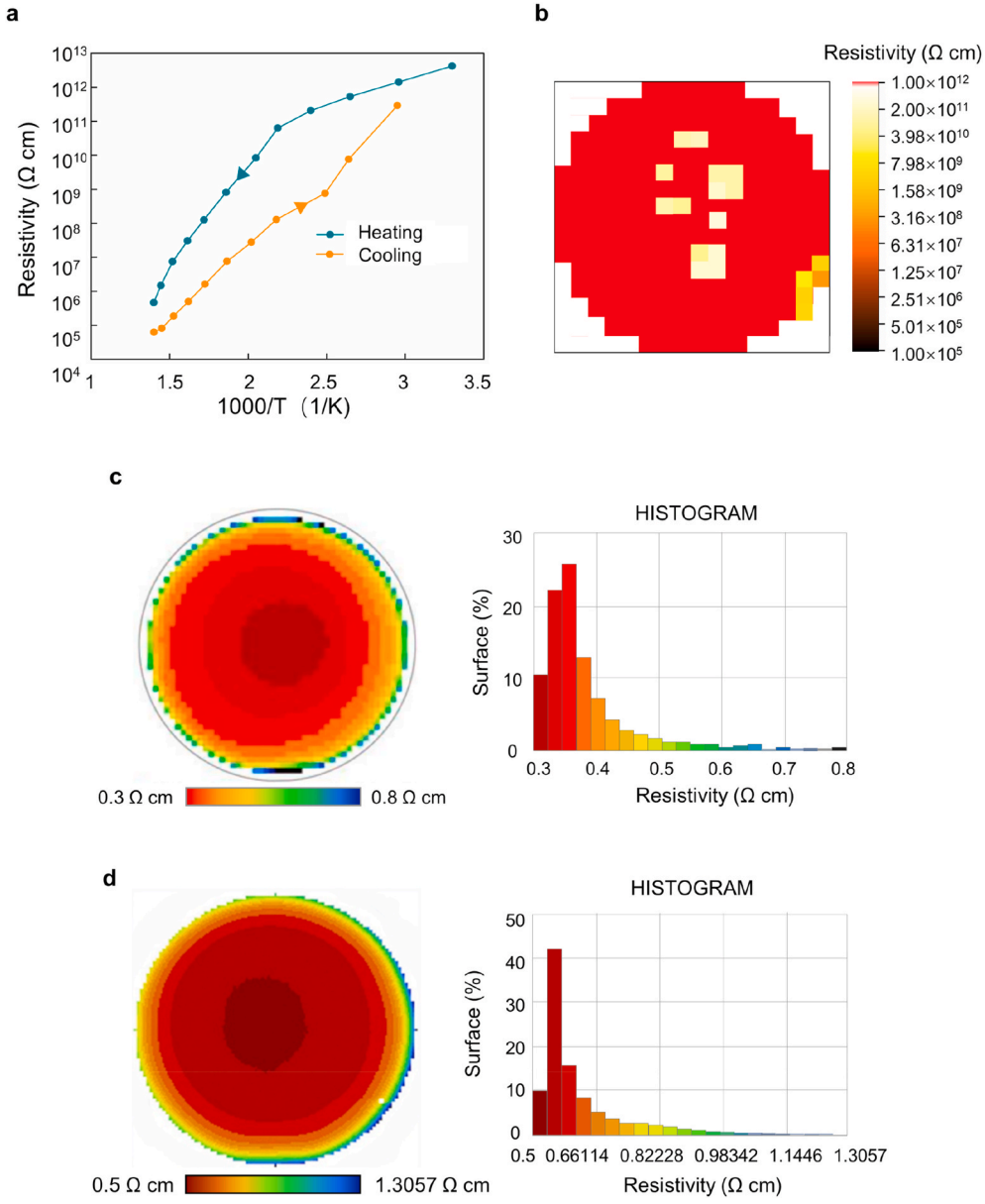

Fig. 4. The resistivity images measured by various electrical methods. a, Resistivity of bulk semi-insulating 4H–SiC determined by van der Pauw measurement while cooling and heating. Reproduced from Ref. [40], copyright 2012, IEEE. **b**, Mapping of the resistivity distribution in V-doped semi-insulating 4H–SiC substrate by using COREMA-WT (red indicates resistivity higher than 10^{12}Ωcm). Reproduced from Ref. [41], copyright 2020, Springer Nature. **c**, Resistivity mapping of a p-type 4H–SiC wafer with the histogram of resistivity occupancy ratio. Reproduced from Ref. [43], copyright 2020, IEEE. **d**, Resistivity mapping for an Al–B co-doped 4H–SiC wafer with the histogram of resistivity occupancy ratio. Reproduced from Ref. [44], copyright 2019, Elsevier B.V.

SiC, the carrier concentration is the difference between the concentration of doped donor impurities and acceptor impurities. All in all, this section will go into great detail regarding the electrical measurement of the SiC carrier concentration.

The average carrier concentration of SiC wafers can be determined by the capacitance-voltage (C–V) method as well as the Hall effect method, which are traditional characterization techniques for determining carrier concentration. For the C–V method, a space charge region is essential as it needs to create a junction capacitance in SiC. Typically, the conventional non-invasive method is the mercury probe Hg-CV with liquid Hg–SiC contact [45,46]. There is a linear relationship between 1/C [2] and the voltage applied in the diode, and the slope of the 1/C [2] versus voltage plot can be used to determine the carrier concentration of SiC (Fig. 5) [47]. As the detection depth of the C–V method is determined by depletion region width, a deeper profile of carrier concentration in SiC can be detected with the increase of applied voltage and the decrease of doping concentration according to the theory in the modulation of the depletion region thickness [48]. It is worth noting that the carrier concentration obtained by the C–V method is the active carrier concentration and may not be equal to doping concentration. Moreover, the C–V method only has a detection limit of 1×10^{19} cm^{-3} as higher doping can lead to the formation of ohmic contact.

For the Hall effect measurement, it is possible to characterize carrier concentration, carrier type, mobility as well as the functional relationship between carrier concentration and temperature [51]. To do the Hall effect measurement, the test sample needs to meet the requirement on ohmic contact. Fortunately, the ohmic contact process of n-type SiC is becoming more mature with the progress of technology [52]. For instance, it has been reported that tantalum(Ta) is used to form an ohmic contact with SiC at high temperatures to suit for the Hall effect measurement [53]. Additionally, a more sophisticated method known as Differential Hall effect (DHE) measurement can be used to determine the spatially distributed carrier concentration.

3.2. *Electrical scanning probe techniques*

Including scanning capacitance microscopy (SCM), scanning spreading resistance microscopy (SSRM), and conductive atomic force microscopy (C-AFM), in recent years, the electrical scanning probe techniques based on atomic force microscopy have been developed to

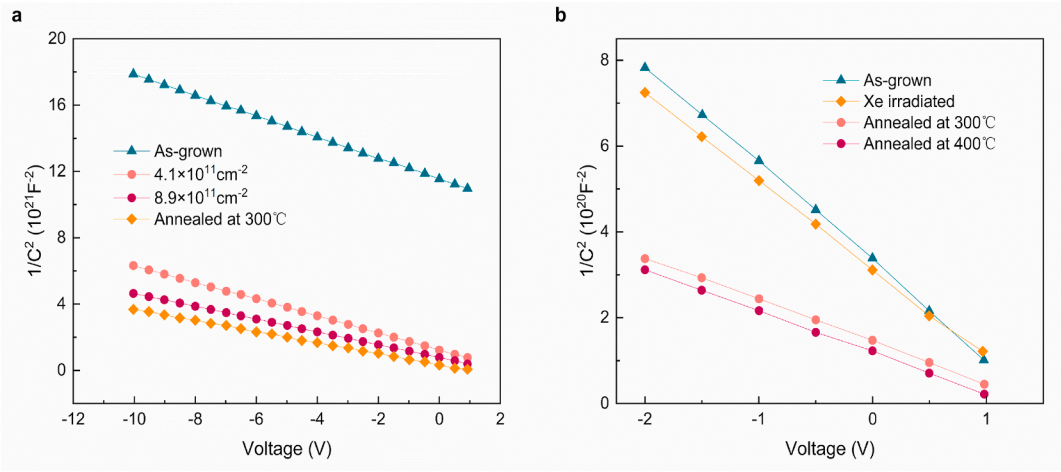

Fig. 5. The C–V measurements of diverse 4H–SiC samples. a, $1/C^2$ versus voltage characteristics of Schottky diodes manufactured on as-grown, irradiated with 5.4 MeV alpha-particles at fluence $4.1 \times 10^{11}cm^{-2}$, $8.9 \times 10^{11}cm^{-2}$, and after annealing at 300 °C for 20min in flowing argon, measured at 300 K. Reproduced from Ref. [49], copyright 2016, Elsevier B.V. **b,** $1/C^2$ versus voltage characteristics of Schottky diodes manufactured on as-grown and Xe ion irradiated before and after isochronally annealing at 300 °C and 400 °C, measured at 300 K. Reproduced from Ref. [50], copyright 2022, Springer Nature.

characterize the 2D distribution of electrical characteristics of SiC (4H,6H,3C) materials and subsequent devices in nanoscale [54–56]. The SCM is based on differential capacitance measurements, which are used to estimate carrier concentration from the signal of dC/dV. Besides, for SSRM, the signal of it is proportional to log(I/V), which reflects the spreading resistance or resistivity of SiC underneath the probe tip. As a result, the SCM is suitable for measuring low carrier concentration samples and the SSRM is for high carrier concentration [57]. In addition, the C-AFM is aimed at measuring current signals to reflect the electrical homogeneity as a qualitative characterization technique [58]. As high-resolution and precise measurement methods, these electrical scanning probe techniques are strongly affected by various defects, morphological features and surface contaminations. Moreover, for measuring high dopant concentration samples, it is necessary to consider the deviation of electrical characteristics affected by impurities ionizing, resulting in high current generated from the tiny probe tip particularly at high temperature [59].

The SCM measurement presents the value of *dC/dV* as the primary signal, which is measured between the probe and oxide/SiC or probe and SiC with an ultrahigh-frequency resonance of capacitance. Similar

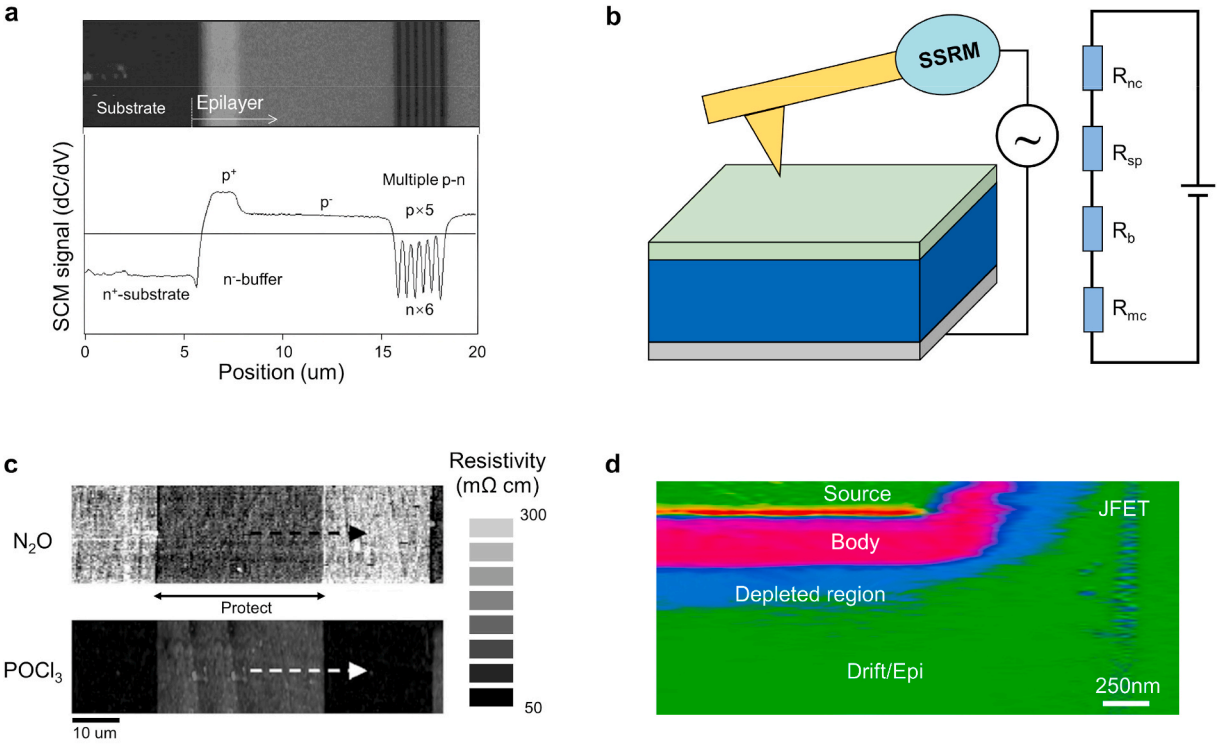

Fig. 6. Electrical scanning probe measurement images. a, Cross-sectional SCM mapping of SiC multiple-pn-junction structure with its line profile. Reproduced from Ref. [60], copyright 2002, IOP Publishing. **b**, 3D schematic illustration of SSRM setup and its equivalent circuit. **c**, Resistivity lateral distribution images measured by SSRM of p-type SiC surface regions subjected to N_2O and $POCl_3$ POA. Reproduced from Ref. [62], copyright 2012, AIP Publishing LLC. **d**, Cross section SCM mapping of an elementary MOSFET cell. Reproduced from Ref. [69], copyright 2021, MDPI.

to C–V measurement, the type and concentration of the majority carrier can be respectively deduced from the positive or negative phase and amplitude of the signal presented. Fig. 6a shows a cross-sectional SCM image and line profile, in which the positive signal corresponds to p-type and the lower amplitude signal corresponds to lower carrier concentration [60]. For SSRM, the signal reflects the magnitude of spreading resistance, from which the resistivity of the regions underneath the probe tip can be calculated. Fig. 6b illustrates the equivalent circuit of SiC in the SSRM measuring, consisting of several contributions such as the tip/SiC nano-contact resistance (R_{nc}), the spreading resistance (R_{sp}) of SiC near the surface region, the resistance of SiC bulk (R_b) and macroscopic back-contact resistance (R_{mc}). In particular, only R_{nc} and R_{sp} vary with the tip position, and the others are constant terms [61]. It is worth noting that, for high doping concentration samples, the carrier concentration of SiC contacted to the tip is high enough to guarantee R_{nc} is a low-resistance Ohmic contact. As a result, the R_{sp} becomes the dominant one and then the resistivity (ρ) can be calculated from the SSRM signal, due to R_{sp} becomes directly proportional to $\rho/4r$, where r is the contact radius [62].

These electrical scanning probe techniques have been explored for a lot of applications related to the doping of SiC. For example, Fiorenza et al. used SCM and SSRM to determine the doping distribution of SiC and use these data to help modify the electronic quality of the SiO_2/SiC interface after post-oxidation-annealing (POA) in nitrides or phosphides ambient [62–64]. As shown in Fig. 6c, the effect of POA with dopants on the net carrier concentration in p-type SiC is apparent from resistivity mapping [62]. In recent years, Giannazzo et al. had used these techniques to measure the 2D distribution of dopants in ion implanted SiC and then investigated the evolution of electrically active dopants with thermal annealing process [65–67]. In addition, a common application of these techniques is to monitor the channel shape and length or electrical junction position in transistor devices like MOSFET and Super-junction [68,69]. Fig. 6d shows a typical cross-section SCM image to reveal the channel shape of elementary MOSFET cell [69]. It has to be emphasized that AC bias may affect the estimation of the channel length. Hence, minimizing the noise/signal ratio and optimizing the bias conditions are essential before formal measuring.

All in all, the electrical characterization methods can both measure the resistivity and carrier concentration, which are closely related to the characteristics of SiC wafers. However, almost all electrical methods only produce average results, making it challenging to determine how the electrical parameters are distributed in SiC wafers. The electrical scanning probe techniques have achieved great success in measuring electrical characteristics distribution of SiC in nanoscale, but with shortcomings of small detection scope and being time-consuming. In addition, some methods such as the C–V method are inconvenient due to the complicated sample preparation process. As a result, it is necessary to develop a fast and convenient characterization technique for determining the distribution of doping concentration in SiC.

4. Optical methods

The above-mentioned methods for elemental analysis and electrical characterization have the shortcomings of being time-consuming and destructive in sample preparation, making them inapplicable for wafer-scale in-line characterization. Moreover, it is challenging to obtain a high-resolution mapping image to determine the homogeneity of doping by electrical characterization on a large scale. Therefore, it is crucial to develop a fast and non-destructive characterization technique. In the past decades, the optical methods, including optical absorption method, Raman spectra analysis and photoluminescence spectroscopy, have gradually become the most common and powerful tools to detect various impurities and intrinsic defects in SiC. The fundamental mechanism behind optical methods is, in general, to connect the characteristic parameters taken from the optical spectra with the electrical characteristics related to the impurities. As a result, almost all optical methods are indirect characterization techniques that require the standard samples to be calibrated for quantitative analysis. More details about optical methods will be discussed in this section.

4.1. Optical absorption method

Optical absorption method is a conventional optical method. The optical absorption method uses the relationship between the optical absorption coefficient (α) and doping levels of 4H–SiC [70] to calculate the carrier concentration, as the peak of free electron correlated absorption peaks are linearly proportional to the carrier concentration. Fig. 7a and b, respectively, show the optical absorption curves of SiC and the linear relationship between absorption peak maximum and the carrier concentration. The basic mechanism is that after absorbing light energy, the electrons jump from the valence band or impurity band to the conduction band. As a result, the absorption intensity rises as the carrier concentration increases. To get the exact experimental result, optical absorption measurement and the Hall effect measurement are utilized to determine the absorption peak and carrier concentration of graded doping SiC samples, respectively, as calibration work. Then the relationship between the carrier concentration and the peak absorption can be calculated and applied to subsequent measurements. The measurement range of carrier concentration of SiC measured by this sort of method is supposed to be within 10^{17}–10 [20] cm^{-3}. If the doping concentration is too low the absorption peak is too weak to detect.

Based on optical absorption spectroscopy, absorption mapping analysis can be carried out to obtain an intuitive spatial carrier level distribution image [71]. Fig. 7c and d show the charge carrier concentration mapping of 4H–SiC and 6H–SiC respectively, and the doping homogeneity in SiC is obvious. The black areas in the middle of the mapping images indicate that the carrier concentration is too high and the incident light is absorbed so that it cannot pass through. In other words, the carrier concentration value in the black area exceeds the detection limit. This method determines the ionized concentration of incorporated impurities, and the original doping concentration can as well be obtained through the ionization degree relationship [72]. Although the accuracy of optical absorption characterization is comparable to that of the Hall effect method, its equipment is cumbersome and expensive, and consequently optical absorption method is restricted for commercialization [73].

Optical transmission spectroscopy is an alternative method to obtain carrier concentration. Based on the transmission measurements, Joshua et al. [75] used the commercially available optical scanner to image the free carrier concentration. There is a good calibration fit between doping concentration and [ln(RGB/255)]/t from several 4H–SiC substrates at different doping concentration levels, as shown in Fig. 8a. Using the calibration curve, Joshua et al. calculated free carrier concentration through the luminosity (RGB value) from the scanner images. As presented in Fig. 8b, the calculated free carrier concentration profile map is obtained using the transmission measurement. The image of carrier concentration distribution shows a good correlation with the Lehighton resistivity map shown in Fig. 8c.

4.2. Raman spectra analysis

Raman scattering microscopy has been used to determine the carrier concentration of SiC with the correspondence between the carrier concentration of SiC and the peak parameters of Raman spectroscopy. Raman scattering is an optical technique to detect vibrations of molecules based on inelastic scattering of light [76]. A_1, E_1 and E_2 modes are Raman-active modes of SiC. Among them, A_1 and E_1 phonon modes, which are also infrared (IR) active, are split into longitudinal optical (LO) and transverse optical (TO) modes. A clear correspondence between A_1 (LO) phonon peak position and nominal carrier concentration was found in nitrogen-doped SiC [77]. In addition, the damping constant of the LO phonon varies linearly with carrier concentration as reported

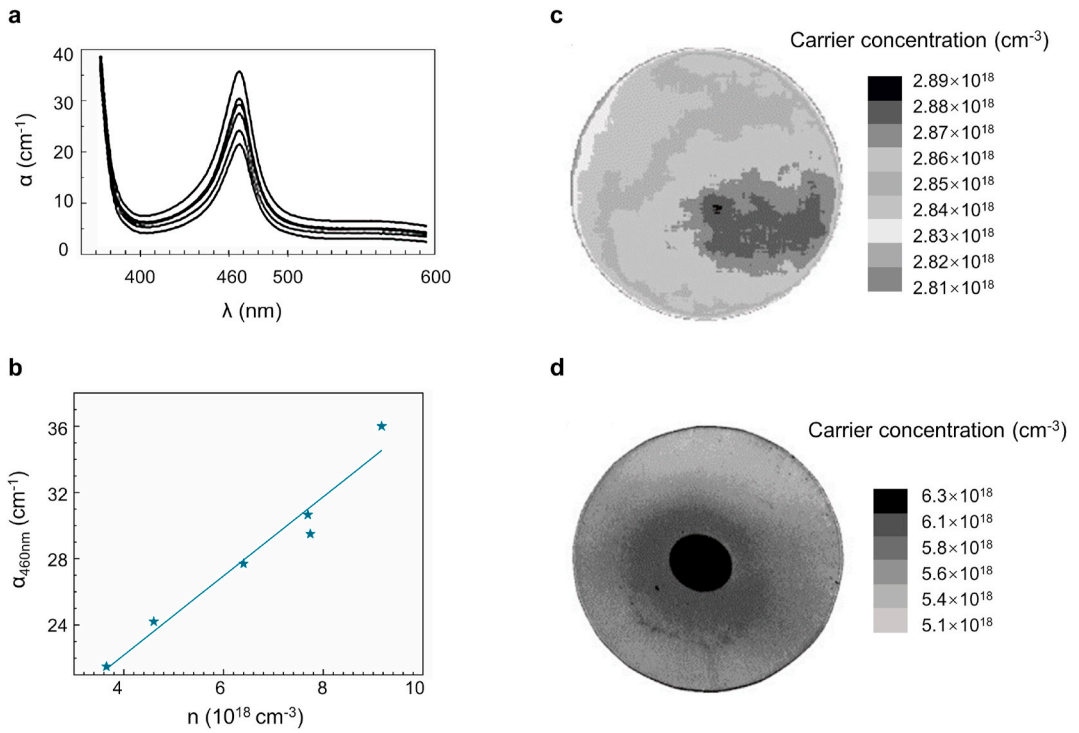

Fig. 7. Optical absorption measurement images. a, Absorption measurement of a series of n-type 4H–SiC. **b**, Calibration curve, linear relationship of absorption peak maximum and charge carrier concentration. Reproduced from Ref. [74], copyright 2001, Elsevier B.V. **c**, Charge carrier concentration mapping of n-doped 4H–SiC. **d**, Charge carrier concentration mapping of n-doped 6H–SiC. The gray levels correspond to carrier concentrations in cm^{-3}. Reproduced from Ref. [71], copyright 2003, Elsevier B.V.

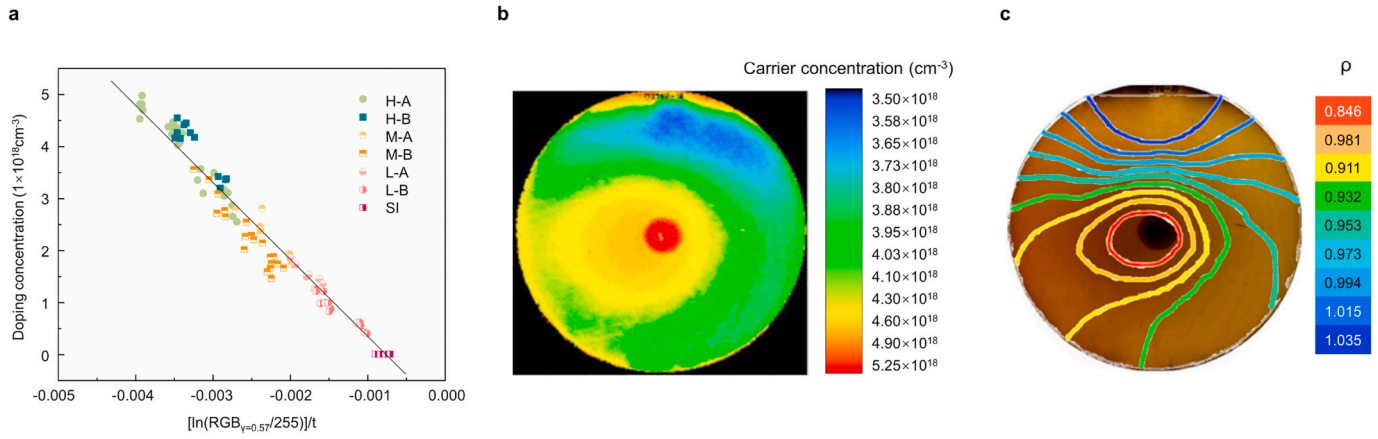

Fig. 8. Optical transmission measurement images. a, Calibration fit from high-doped (H), moderate doped (M), low doped (L) and semi-insulating (SI) 4H–SiC samples from both A and B vendors. of n-type 4H–SiC. **b**, Mapping of free carrier concentration for 2-inch sample CO246-19. **c**, Overlay of Lehighton ρ mapping of the sample upon a contrast-enhanced transmission image of CO246-19. Reproduced from Ref. [75], copyright 2007, AIP Publishing LLC.

in previous papers [62]. As shown in Fig. 9, the damping constant is linearly related to the carrier concentration for graded doping samples A, B and C.

The mechanism for the Raman shift of LO mode above is the coupling interaction between LO phonons and the overdamped plasmons. However, the longitudinal optical plasmon coupling (LOPC) mode in SiC has received more attention in research, since the TO phonon band is insensitive to free carriers in most cases [61]. The frequency shift of the LOPC mode and line shapes such as full width at half maximum (FWHM) were frequently used to estimate the carrier concentration [78]. For instance, a frequency shift of LOPC mode in n-type 4H–SiC can be observed with varied carrier concentration [79,80]. Fig. 10a shows a shift of Raman characteristic peak of n-type 4H–SiC with different carrier concentrations. In LOPC mode, the carrier concentration in a range from 10^{16} cm^{-3} to 10^{19} cm^{-3} can be estimated from the peak frequency [81,82]. Additionally, in p-type SiC, the relationship between the FWHM of the characteristic peak of Raman spectra and the carrier concentration in SiC bulk wafers was found (Fig. 10b). In Al-implanted 4H–SiC, the LO+ Raman peak (~980 cm^{-1} – 1000 cm^{-1}) showed a left shift towards the LO peak, indicating an increase in free carrier concentration [83]. Furthermore, for heavily doped SiC, a great deal of attention has been devoted to the analysis of the Fano interference effect between the folded transverse acoustic (FTA) phonon modes and the continuum of electronic transitions [84,85]. For example, the asymmetric parameters were used to determine the hole concentration in 4H–SiC [78], with a sensitivity up to 10^{18} cm^{-3}.

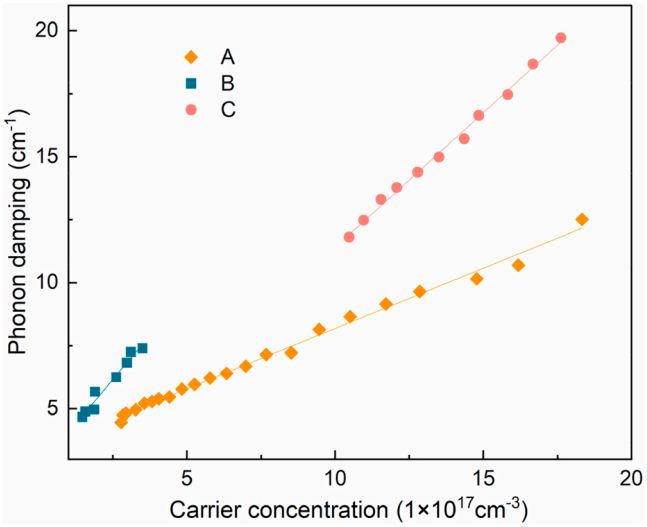

Fig. 9. LO phonon damping of Raman spectra from 4H–SiC. The damping constant of the LO phonon is plotted as a function of the carrier concentration for graded doping samples (A, B and C). Reproduced from Ref. [61], copyright 2008, AIP Publishing LLC.

The carrier concentration of SiC with graded doping levels is measured for calibration by the Hall effect measurement first, and then the carrier concentration and peak parameters such as FWHM of the Raman spectra characteristic peak is to be determined by performing a curve fitting. Raman imaging analysis can be used to determine the higher carrier concentration of single-crystal SiC upmost compared with the optical absorption characterization. However, as the concentration increases, the signal-to-noise ratio goes down [86]. Fortunately, it has been found recently that SiC with lower carrier concentrations can be detected when using an excitation source with energy higher than the band gap of 4H–SiC [87]. In addition, a novel Raman scattering characterization technique for estimating nitrogen doping concentration in heavily N-doped ($>1 \times 10^{19}$cm^{-3}) 4H–SiC is proposed. This technique makes use of the integrated intensity of the LOPC mode signal arising at 1100 cm^{-1} and has a higher sensitivity for measuring nitrogen concentration than the conventional characterization techniques that make use of the LOPC peak shift and the Fano interference effect [88].

Raman mapping is an imaging scan technique that employs point-to-point scanning to measure adjacent sample micro-regions sequentially. The carrier concentration in every micro-region of SiC wafers can be calculated with the curve fitting to construct the Raman spectral mapping, which is named spatially resolved Raman measurement [89]. Fig. 10c displays a carrier concentration mapping of n-type (nitrogen and boron co-doped) 4H–SiC wafer based on the relationship between the carrier concentration and the frequency shift in LOPC mode [90]. Fig. 10d shows a hole concentration mapping of a 2-inch highly Al-doped 4H–SiC based on the analysis of Raman spectra using the calibration curve of the asymmetry parameter in FTA mode [85]. In addition, confocal Raman spectroscopy has been employed as a novel technique to obtain depth profiling of carrier concentration in SiC [91], and the schematic of the measurement process is shown in Fig. 11.

4.3. Photoluminescence spectroscopy

Photoluminescence spectroscopy is a frequently used method to obtain carrier concentration. The photoluminescence spectroscopy (PL) of the impurities at the substitute site exhibits various sharp lines as a result of the recombination of bound excitons (BE) at these impurities, such as boron acceptors and nitrogen donors [92]. Thus, different from

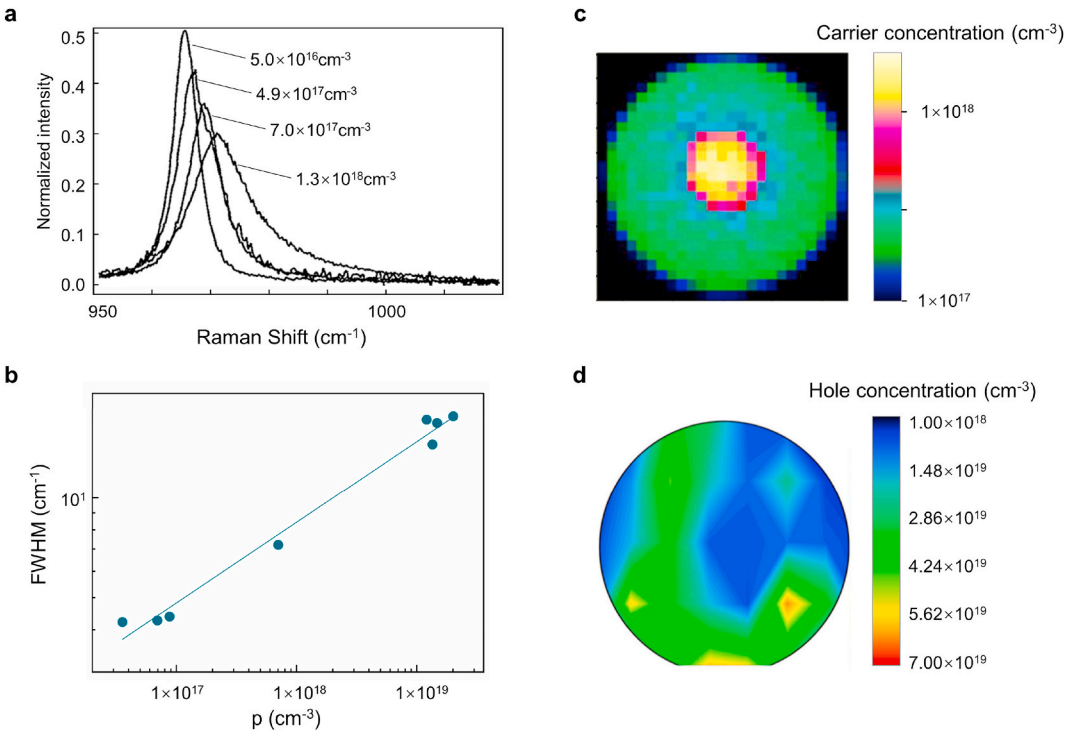

Fig. 10. Raman spectra analysis in LOPC modes. a Raman profiles of LOPC mode for 4H–SiC with different carrier concentrations. Reproduced from Ref. [80], copyright 1995, AIP Publishing LLC. **b**, Calibration plot of A1-(LOPC) Raman line width versus charge carrier concentration of aluminum doped p-type 6H–SiC ((0001) oriented wafer). The charge carrier concentration was determined using Hall measurements. Reproduced from Ref. [86], copyright 2005, Trans Tech Publications Ltd. **c**, Simulated carrier concentration distribution of 2-inch nitrogen-boron doped 4H–SiC by Raman analysis. The interval mapping point is 2 mm. Reproduced from Ref. [90], copyright 2013, ESG. **d**, Hole concentration mapping of 2-inch highly Al-doped 4H–SiC by Raman analysis in FTA mode. Reproduced from Ref. [85], copyright 2015, Trans Tech Publications Ltd.

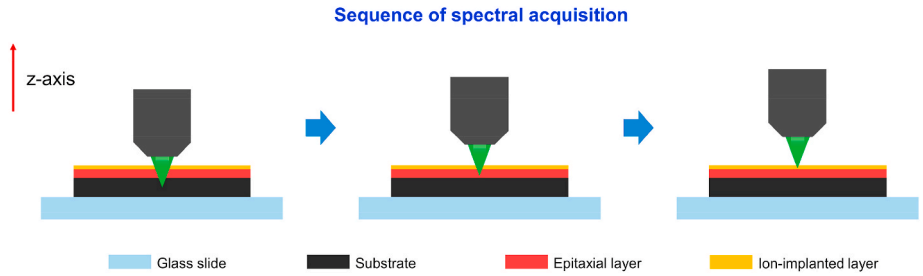

Fig. 11. Confocal Raman spectroscopy. Schematic of the depth profiling. Reproduced from Ref. [91], copyright 2020, MDPI.

Raman spectra, PL spectra exhibit a shift in emission intensity rather than a shift in peak position or FWHM caused by variations of doping concentration in SiC [90]. This sort of characteristic in PL spectra is more helpful for measuring impurity concentration in single-crystal SiC.

As shown in Fig. 12a, the linear relationship between nitrogen doping concentration and the ratio (R) of the line peak intensity of the nitrogen-bound excitons (BE) to the free excitons (FE), has been found in the low-temperature photoluminescence (PL) spectroscopy of uncompensated nitrogen-doping n-type 4H–SiC and 6H–SiC [93]. Nevertheless, as the FE lines can only be observed in n-type 4H–SiC when doping

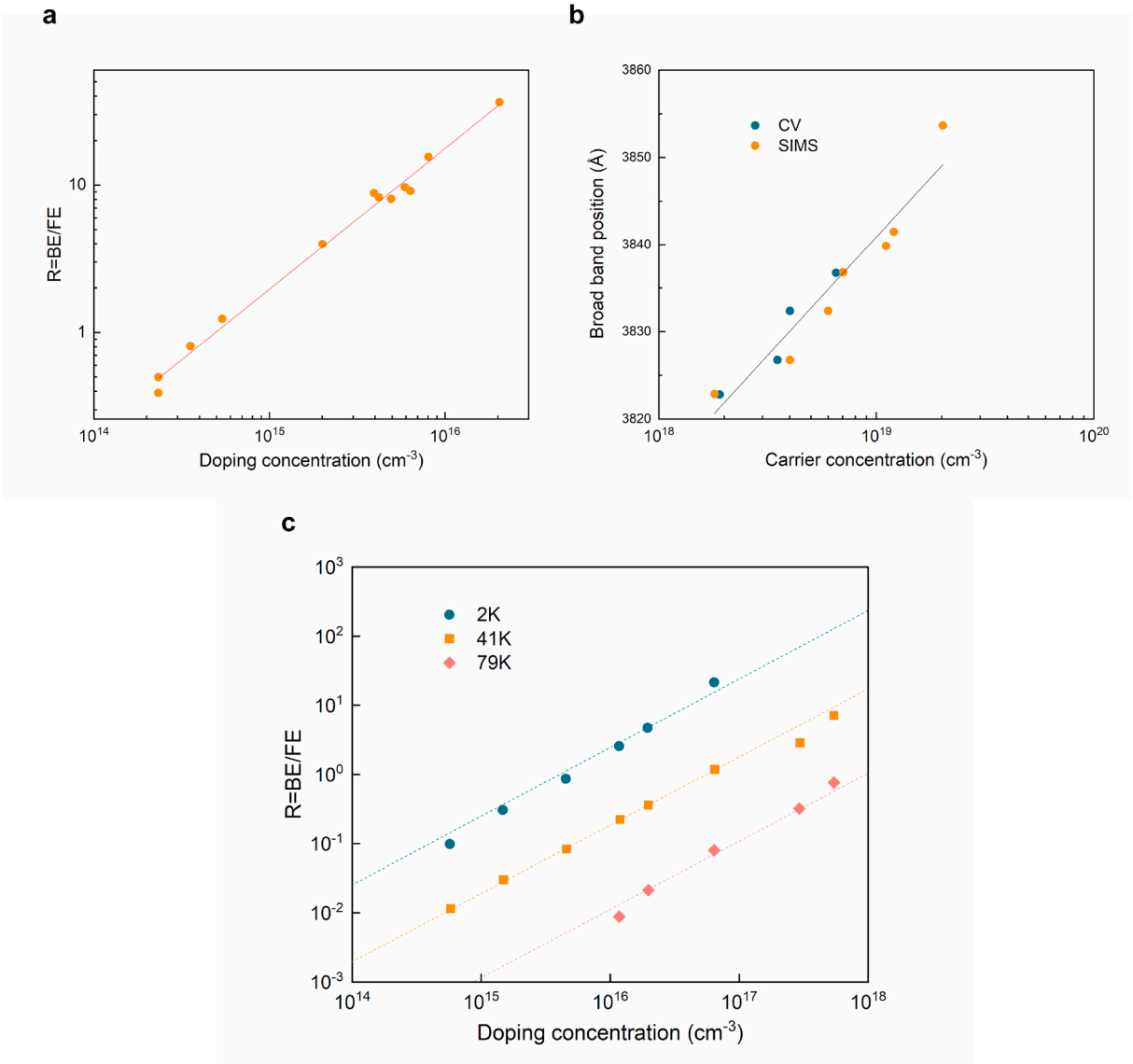

Fig. 12. Photoluminescence spectroscopy. a, The logarithmic plot of the ratio R (BE/FE) versus the carrier concentration of 4H–SiC determined by C–V. Reproduced from Ref. [93], copyright 1996, AIP Publishing LLC. **b**, The linear relationships between the broad band (BB) energy position shift and the net carrier concentration obtained by CV or nitrogen atomic concentration as determined with SIMS. Reproduced from Ref. [92], copyright 2005, IOP Publishing. **c**, The ratio R (BE/FE) as a function of the aluminum doping concentration obtained from 4H–SiC substrates at three different temperatures (2 K, 41 K, 79 K). Reproduced from, copyright 2017, AIP Publishing LLC.

concentration is lower than 3×10^{16} cm^{-3}, it is necessary to concentrate on other characteristics of PL spectra. Henry et al. discovered a useful calibration curve of broad band (BB) energy position versus the doping concentration in the doping range of more than 3×10^{18} cm^{-3} and the associated spectrum is shown in Fig. 12b· [92]. A similar finding for the relationship between doping concentration and R in Al-doping p-type 4H–SiC was presented in Fig. 12 c [94]. It should be noted that the sensitivity of PL spectroscopy will have a negative effect on R. As the temperature rises, the sensitivity of PL will decrease. The PL method can be used to determine the carrier concentration of SiC crystals over a wide range, even down to 10^{13} cm^{-3} [95]. Additionally, Glaser et al. discovered a linear correlation between the intensity of specific distinguishing PL line peaks (SN1, Vc-Vsi) and the carrier concentration in single-crystal SiC [96]. However, Rusheng et al. proved that in nitrogen-doped 4H–SiC, the intensity of the distinct PL peak at 538 nm (2.3 eV) did not increase linearly with the doping concentration because of donor-acceptor pair recombination and free carrier absorption [90]. In addition, the characterization on doping can be affected by the electrically active defects due to the compensation effect of those defects in SiC. As a result, accurate detection of certain defects may aid in the characterization of doping concentration.

At present, the PL mapping technique is primarily used to qualitatively characterize various defects in SiC [97,98], and there are a low number of examples of successful applications to quantitatively determine its carrier concentration [99,100], probably because of the low efficiency of PL in characterizing indirect band gap materials such as SiC. Moreover, a quantitative correlation between the PL peaks and the carrier concentration is more obscure when there are many specific impurities in SiC. Nevertheless, the PL measurement method at low temperature has unique advantages, such as a higher resolution due to a much smaller size of the exciting-laser spot compared to other optical methods. In addition, it was demonstrated that the mapping image of the infrared photoluminescence of SiC has a good correlation with the resistivity mapping obtained by COREMA [101], which provides certain rationales for determining the resistivity of SiC through the PL mapping technique. Considering the advantage of high resolution and less time-consuming of PL mapping technique, the application of PL mapping in determining carrier concentration and resistivity are worthwhile making further study.

In summary, the PL technique has a good detection limit as low as 10^{13} cm^{-3} and is also suitable for high-doped SiC materials similar to Raman spectra analysis. The PL and optical absorption methods are both fast measurement techniques within several seconds and have nearly the same signal-to-noise ratio [99]. Raman mapping is a time-consuming method as a result of point-to-point scanning and it is not appropriate for in situ diagnostic for SiC wafers, unless using the multi-laser system to measure the whole microregions simultaneously. Moreover, the optical absorption method has the shortcoming of the cumbersome equipment, while the PL method needs to be operated in cryogenic temperatures in the period of measuring, which restricts its application in industrial line. Therefore, it would be worthwhile to develop a novel PL method that can operate at room temperature for in situ diagnostic.

5. Conclusion

This article provides a general overview of three types of characterization methods that can be used to measure the doping of SiC, which are elemental analysis methods, the electrical methods, and the optical methods. SIMS as an elemental analysis method is a powerful method to determine the concentration of all impurities in SiC over a wide detection range, but it is time-consuming and not inapplicable for wafer-scale characterization. For the electrical methods, the non-contact eddy current method and the C–V method are both typical conventional electrical measurement techniques that are able to measure the resistivity and carrier concentration of SiC. Hall effect can as well be used to measure both carrier concentration and resistivity of SiC. In addition, the contactless resistivity mapper techniques have become the mainstream tools to determine the distribution of the resistivity of SiC wafers. Moreover, the electrical scanning probe techniques, developed in recent years, can provide the nano-scale resolution electrical characteristics of SiC materials and subsequent devices.

This article then goes into great detail about the optical absorption technique, Raman spectra analysis, and photoluminescence technique. The detection range of these three optical techniques are 10^{17} cm^{-3} to 10^{20} cm^{-3}, 10^{16} cm^{-3} to 10^{20} cm^{-3} and 10^{13} cm^{-3} to 10^{19} cm^{-3}, respectively. The doping concentration of single-crystal SiC can be estimated from the optical spectra by acquiring the correlated parameters such as peak frequency shift. A competitive advantage of the optical methods is that it can provide the possibility for imaging the doping homogeneity within a moment. But the Raman spectra mapping technique takes a relatively long time due to its point-to-point scanning mode. On the other hand, the PL technique requires cryogenic temperatures during measuring, consequently limiting its application in process monitoring.

The advantages and disadvantages of the three different sorts of characterization methods are concluded as follows. The elemental analysis methods are generally destructive for the SiC samples and can only detect a small region of SiC wafer, making them inapplicable for wafer-scale characterization. The electrical methods are inconvenient because they require the formation of contacts for characterizing the parameters of SiC material. Furthermore, conventional electrical methods can only be used to determine the average values of electrical parameters. The electrical scanning probe techniques are suitable for measuring the distribution of electrical characteristics with high resolution, nevertheless, inapplicable for wafer-scale characterization. Optical methods are fast and non-destructive, but they are indirect and require preliminary calibration with electrical methods like the Hall effect measurement, and it is necessary to improve the accuracy of optical methods. Future works are predicted to favor fast and practical characterization techniques that can be applied into process monitoring such as the non-destructive and non-contact optical methods.

Declaration of competing interest

The authors declare that they have no known competing financial interests or personal relationships that could have appeared to influence the work reported in this paper.

Data availability

No data was used for the research described in the article.

Acknowledgements

The authors would like to acknowledge the funding from the “Pioneer” and “Leading Goose” R&D Program of Zhejiang (2022C01021).

References

[1] Y.C. Huang, et al., High thermal dissipation of normally off P-GaN gate AlGaN/GaN HEMTs on 6-inch N-doped low-resistivity SiC substrate, Micromachines 12 (5) (2021) 509.
[2] J.Y. Jiang, et al., Demonstration of CMOS integration with high-voltage double-implanted MOS in 4H-SiC, IEEE Electron. Device Lett. 42 (1) (2021) 78–81.
[3] Y.K. Sharma, et al., Use of 1.7 kV and 3.3 kV SiC diodes in Si-IGBT/SiC hybrid technology, J. Kor. Phys. Soc. 73 (9) (2018) 1356–1361.
[4] M. Kaneko, T. Kimoto, High-temperature operation of N- and P-channel JFETs fabricated by ion implantation into a high-purity semi-insulating SiC substrate, IEEE Electron. Device Lett. 39 (5) (2018) 723–726.
[5] A. Allca-Pekarovic, et al., Comparison of IGBT and SiC inverter loss for 400V and 800V DC bus electric vehicle drivetrains, in: 2020 IEEE Energy Conversion Congress and Exposition (ECCE), 2020. Conference, Location.

[6] X. Jia, et al., System-level conducted EMI model for SiC powertrain of electric vehicles, in: 2020 IEEE Applied Power Electronics Conference And Exposition (APEC), 2020. Conference, Location.
[7] G. Wolfowicz, et al., Optical charge state control of spin defects in 4H-SiC, Nat. Commun. 8 (1) (2017) 1876.
[8] M. Bathen, et al., Electrical charge state identification and control for the silicon vacancy in 4H-SiC, NPJ Quant. Informat. 5 (2019).
[9] N.T. Son, I.G. Ivanov, Charge state control of the silicon vacancy and divacancy in silicon carbide, J. Appl. Phys. 129 (21) (2021): 215702.
[10] E. Igumbor, et al., Electrically active induced energy levels and metastability of B and N vacancy-complexes in 4H-SiC, J. Phys. Condens. Matter 30 (2018).
[11] N. Iwamoto, B.G. Svensson, Chapter ten - point defects in silicon carbide, in: L. Romano, V. Privitera, C. Jagadish (Eds.), Semiconductors and Semimetals, Elsevier, 2015, pp. 369–407.
[12] K. Tsunenobu, A.C. James, Appendix C: major physical properties of common SiC polytypes, in: Fundamentals of Silicon Carbide Technology: Growth, Characterization, Devices and Applications, IEEE, 2014, pp. 521–524.
[13] M. Bickermann, et al., Incorporation of boron and vanadium during PVT growth of 6H-SiC crystals, J. Cryst. Growth 233 (1) (2001) 211–218.
[14] Y.M. Tairov, V.F. Tsvetkov, General principles of growing large-size single crystals of various silicon carbide polytypes, J. Cryst. Growth 52 (1981) 146–150.
[15] T. Kimoto, Bulk and epitaxial growth of silicon carbide, Prog. Cryst. Growth Char. Mater. 62 (2) (2016) 329–351.
[16] N.T. Son, et al., Hyperfine interaction of nitrogen donor in 4H-SiC studied by pulsed-ENDOR, Mater. Sci. Forum 483–485 (2005) 351–354.
[17] P. Deák, et al., Some like it shallower" – p-type doping in SiC, Phys. Status Solidi (b) 235 (1) (2003) 139–145.
[18] S.G. Sridhara, et al., Photoluminescence and transport studies of boron in 4H-SiC, J. Appl. Phys. 83 (1998) 7909–7919.
[19] H.M. Hobgood, et al., Semi-insulating 6H-SiC grown by physical vapor transport, Appl. Phys. Lett. 66 (1995) 1364–1366.
[20] S. Song, X.B. Hu, X.G. Xu, Growth and characterization of semi-insulating SiC single crystal, Rengong Jingti Xuebao/J. Synthet. Crystals 41 (2012) 166–169.
[21] D.G. Shin, et al., Impurity behavior of high purity SiC powder during SiC crystal growth, Mater. Sci. Forum 778–780 (2014) 22–25.
[22] W.C. Mitchel, et al., Electrical properties of unintentionally doped semi-insulating and conducting 6H-SiC, J. Appl. Phys. 100 (2006), 043706-043706-5.
[23] D. Schulz, et al., Study of nitrogen incorporation in 6H-SiC single crystals grown by PVT, Mater. Sci. Forum 338–342 (2000) 87–90.
[24] F. Fernández (Ed.), Secondary Ion Mass Spectrometry (SIMS): Principles and Applications Conference, 2012. Location.
[25] D. Feng, et al., Occurrence forms of major impurity elements in silicon carbide, Ceram. Int. 48 (1) (2022) 205–211.
[26] P. Zhao, et al., Study of carbon in thermal oxide formed on 4H-SiC by XPS, Mater. Sci. Forum 483–485 (2005) 653–656.
[27] J. Sameshima, et al., Optimization of the depth resolution for profiling SiO_2/SiC interfaces by dual-beam TOF-SIMS combined with etching, Surf. Interface Anal. 51 (7) (2019) 743–753.
[28] S.I. Soloviev, Y. Gao, T.S. Sudarshan, Doping of 6H–SiC by selective diffusion of boron, Appl. Phys. Lett. 77 (24) (2000) 4004–4006.
[29] P. Konarski, et al., Depth profile Analysis of phosphorus implanted SiC structures, Acta Phys. Pol., A 128 (2015) 864–867.
[30] M.K. Linnarsson, A. Hallén, L. Vines, Intentional and unintentional channeling during implantation of ^{51}V ions into 4H-SiC, Semicond. Sci. Technol. 34 (11) (2019): 115006.
[31] J. Sameshima, et al., Profiling with depth resolution of sub-nm for SiO_2/SiC interface by dual-beam TOF-SIMS combined with simulation, Mater. Sci. Forum 1004 (2020) 587–594.
[32] V.S. Smentkowski, S. Goswami, Quantitative depth profiling of Al in SiC using time of flight–secondary ion mass spectroscopy, J. Vac. Sci. Technol. 39 (3) (2021): 033204.
[33] M. Linnarsson, et al., formation of precipitates in heavily boron doped 4H-SiC, Appl. Surf. Sci. - APPL SURF SCI 252 (2006) 5316–5320.
[34] E. Jung, et al., Synthesis of V-doped SiC powder for growth of semi-insulating SiC crystals, Ceram. Int. 44 (18) (2018) 22632–22637.
[35] Y. Li, Y. Gao, Characterization of SiC materials and devices by SIMS, MRS Proceed. 911 (2006), 911-B05-B20.
[36] A.L. Pivovarov, et al., Optimization of secondary ion mass Spectrometry detection limit for N in SiC, J. Vac. Sci. Technol. 21 (5) (2003) 1649–1654.
[37] L. Wang, B.-S. Park, SIMS analysis of nitrogen in silicon carbide using raster change technique, MRS Online Proc. Libr. 911 (1) (2011) 508.
[38] M. Treu, et al., Challenges and first results of SiC Schottky diode manufacturing using a 3-inch technology, Mater. Sci. Forum 457–460 (2004) 981–984.
[39] P.G. Muzykov, et al., High resistivity measurement of SiC wafers using different techniques, J. Electron. Mater. 32 (6) (2003) 505–510.
[40] K.C. Mandal, et al., Characterization of 4H-SiC epitaxial layers and high-resistivity bulk crystals for radiation detectors, IEEE Trans. Nucl. Sci. 59 (4) (2012) 1591–1596.
[41] J.Y. Yu, et al., Inhomogeneity of minority carrier lifetime in 4H-SiC substrates, Crystallogr. Rep. 65 (7) (2020) 1231–1236.
[42] Q. Li, et al., Nonuniformities of electrical resistivity in undoped 6H-SiC wafers, J. Appl. Phys. 97 (2005), 113705-113705-6.
[43] G. Zhong, et al., Growth of high quality and low resistivity Φ100mm P-type 4H-SiC single crystal, in: 2020 17th China International Forum on Solid State Lighting & 2020 International Forum on Wide Bandgap Semiconductors China (SSLChina: IFWS), 2020. Conference, Location.
[44] X. Xuejian, et al., Sublimation growth and property characterization of P-type 4H-SiC by AlB Co-doping technique, Scripta Mater. 167 (2019) 76–80.
[45] A. Savtchouk, et al., Accurate doping density determination in SiC with constant surface potential corona charging; industry ready alternative to Hg-CV, Mater. Sci. Forum 858 (2016) 509–512.
[46] L. Zhao, H. Wu, A correlation study of substrate and epitaxial wafer with 4H-N type silicon carbide, J. Cryst. Growth 507 (2019) 109–112.
[47] A. Ruggiero, et al., Effects of implantation defects on the carrier concentration of 6H-SiC, Appl. Phys. A 82 (3) (2006) 543–547.
[48] K. Fukada, et al., Depth profile of doping concentration inthick (> 100 μm) and low-doped (< 4 × 1014 Cm−3) 4H-SiC epilayers, in: 2016 European Conference on Silicon Carbide & Related Materials (ECSCRM), 2016. Conference, Location.
[49] E. Omotoso, et al., Electrical characterization of deep levels created by bombarding nitrogen-doped 4H-SiC with alpha-particle irradiation, Nucl. Instrum. Methods Phys. Res. Sect. B Beam Interact. Mater. Atoms 371 (2016) 312–316.
[50] E. Omotoso, et al., DLTS study of the influence of annealing on deep level defects induced in xenon ions implanted N-type 4H-SiC, J. Mater. Sci. Mater. Electron. 33 (19) (2022) 15679–15688.
[51] S. Contreras, et al., Results of SIMS, LTPL and temperature-dependent Hall effect measurements performed on Al-doped α-SiC substrates grown by the M-PVT method, Mater. Sci. Forum 527–529 (2006) 633–636.
[52] F. Cao, et al., Low temperature Cu/Ti/Al ohmic contacts to P-type 4H-SiC, J. Alloys Compd. 901 (2022): 163580.
[53] W.C. Mitchel, et al., High temperature Hall effect measurements of semi-insulating 4H–SiC substrates, Solid State Electron. 48 (2003) 1693–1697.
[54] F. Giannazzo, et al., Electrical characterization of Al implanted 4H-SiC layers by four point probe and scanning capacitance microscopy, Mater. Sci. Forum 615–617 (2009) 457–460.
[55] X. Song, et al., Structural and electrical characterizations of N-type implanted layers and ohmic contacts on 3C-SiC, Nucl. Instrum. Methods Phys. Res. Sect. B Beam Interact. Mater. Atoms 269 (18) (2011) 2020–2025.
[56] F. Giannazzo, et al., Carrier concentration profiles in 6H-SiC by scanning capacitance microscopy, Mater. Sci. Semicond. Process. 4 (1) (2001) 195–199.
[57] P. Fiorenza, et al., A look underneath the SiO2/4H-SiC interface after N_2O thermal treatments, Beilstein J. Nanotechnol. 4 (2013) 249–254.
[58] T. Sledziewski, et al., Effect of germanium doping on electrical properties of N-type 4H-SiC homoepitaxial layers grown by chemical vapor deposition, J. Appl. Phys. 120 (20) (2016): 205701.
[59] J. Osterman, A. Hallén, S. Anand, Carrier profiling of Al-doped 4H-SiC by scanning spreading resistance microscopy, Appl. Phys. Lett. 81 (16) (2002) 3004–3006.
[60] J. Suda, et al., Scanning capacitance and spreading resistance microscopy of SiC multiple-pn-junction structure, Jpn. J. Appl. Phys. 41 (1A) (2002) L40.
[61] F. Giannazzo, et al., Highly homogeneous 2D/3D heterojunction diodes by pulsed laser deposition of MoS2 on ion implantation doped 4H-SiC, Adv. Mater. Interfaces (2022) 2201502. N/a(n/a).
[62] L.K. Swanson, et al., Correlating macroscopic and nanoscale electrical modifications of SiO_2/4H-SiC interfaces upon post-0xidation-annealing in N_2O and $POCl_3$, Appl. Phys. Lett. 101 (19) (2012): 193501.
[63] P. Fiorenza, et al., Nanoscale probing of the lateral homogeneity of donors concentration in nitridated SiO_2/4H–SiC interfaces, Nanotechnology 27 (2016).
[64] P. Fiorenza, et al., SiO_2/4H-SiC interface doping during post-deposition-annealing of the oxide in N_2O or $POCl_3$, Appl. Phys. Lett. 103 (15) (2013): 153508.
[65] Q. Jin, et al., Lateral spreads of ion-implanted Al and P aAoms in silicon carbide, Jpn. J. Appl. Phys. 60 (2021).
[66] F. Giannazzo, et al., Effect of Thermal Annealing on the Electrically Active Profiles and Surface Roughness in Multiple Al Implanted 4H-SiC, in: 2007 15th International Conference on Advanced Thermal Processing of Semiconductors, 2007. Conference, Location.
[67] F. Giannazzo, et al., Nanoscale characterization of SiC interfaces and devices, Mater. Sci. Forum 778–780 (2014) 407–413.
[68] R. Kosugi, et al., Development of SiC super-junction (SJ) device by deep trench-filling epitaxial growth, Mater. Sci. Forum 740–742 (2013) 785–788.
[69] P. Fiorenza, et al., High-resolution two-dimensional imaging of the 4H-SiC MOSFET channel by scanning capacitance microscopy, Nanomaterials 11 (6) (2021) 1626.
[70] G.B. Dubrovskii, A.A. Lepneva, E.I. Radovanova, Optical absorption associated with superlattice in silicon carbide crystals, Phys. Status Solidi 57 (1) (1973) 423–431.
[71] P.J. Wellmann, R. Weingärtner, Determination of doping levels and their distribution in SiC by optical techniques, Mater. Sci. Eng., B 102 (1) (2003) 262–268.
[72] D. Firsov, et al., Evaluation of nitrogen incorporation into bulk 4H-SiC grown on seeds of different orientation from optical absorption spectra, J. Phys. Conf. 741 (2016): 012043.
[73] J.D. Caldwell, et al., SiC substrate doping profiles using commercial optical scanners, Mater. Sci. Forum 527–529 (2006) 725–728.
[74] R. Weingärtner, et al., Absorption mapping of doping level distribution in N-type and P-type 4H-SiC and 6H-SiC, Mater. Sci. Eng., B 80 (1) (2001) 357–361.
[75] J. Caldwell, et al., Free carrier distribution profiling of 4H-SiC substrates using a commercial optical scanner, J. Appl. Phys. 101 (2007), 093506-093506.
[76] M. Chafai, et al., Micro-Raman and Hall effect study of N-type bulk 4H-SiC, Mater. Sci. Forum 338–342 (2000) 707–710.
[77] J.C. Burton, et al., Spatial characterization of doped SiC wafers by Raman spectroscopy, J. Appl. Phys. 84 (11) (1998) 6268–6273.

[78] S. Juillaguet, et al., Raman investigation of aluminum-doped 4H-SiC, Mater. Sci. Forum 740–742 (2013) 357–360.
[79] M. Chafai, et al., Raman scattering from LO phonon-plasmon coupled modes and Hall-effect in N-type silicon carbide 4H-SiC, J. Appl. Phys. 90 (2001) 5211–5215.
[80] H. Harima, S.i. Nakashima, T. Uemura, Raman Scattering from Anisotropic LO-phonon–plasmon–coupled Mode in N-type 4H– and 6H–SiC, J. Appl. Phys. 78 (3) (1995) 1996–2005.
[81] S. Nakashima, et al., Determination of free carrier density in the low doping regime of 4H-SiC by Raman scattering, Appl. Phys. Lett. 93 (12) (2008): 121913.
[82] S. Nakashima, et al., Raman scattering study of carrier-transport and phonon properties of 4H-SiC crystals with graded doping, Phys. Rev. B 76 (24) (2007): 245208.
[83] Z.W. Xu, et al., Raman spectroscopy characterization of ion implanted 4H-SiC, Mater. Sci. Forum 963 (2019) 424–428.
[84] T. Mitani, et al., Determination of carrier concentration by Fano interference of Raman scattering in heavily doped N-type 4H-SiC, J. Appl. Phys. 112 (4) (2012): 043514.
[85] P. Kwasnicki, et al., Raman investigation of heavily Al doped 4H-SiC layers grown by CVD, Mater. Sci. Forum 806 (2015) 51–55.
[86] P.J. Wellmann, et al., Micro-optical characterization study of highly P-type doped SiC:Al wafers, Mater. Sci. Forum 483–485 (2005) 393–396.
[87] T. Liu, et al., Raman characterization of carrier concentrations of Al-implanted 4H-SiC with low carrier concentration by photo-generated carrier effect, Crystals 9 (2019) 428.
[88] K. Yokomoto, et al., Novel characterization method for the nitrogen doping concentration in heavily nitrogen-doped 4H-SiC cystals by Raman scattering microscopy, Jpn. J. Appl. Phys. 59 (5) (2020): 051003.
[89] M. Mermoux, A. Crisci, F. Baillet, Raman imaging analysis of SiC wafers, Mater. Sci. Forum 433–436 (2003) 353–356.
[90] R. Wei, et al., Characterization of nitrogen-boron doped 4H-SiC substrates, Int. J. Electrochem. Sci. 8 (2013) 7099–7106.
[91] Y. Song, et al., Depth profiling of ion-implanted 4H–SiC using confocal Raman spectroscopy, Crystals 10 (2) (2020) 131.
[92] A. Henry, et al., Determination of nitrogen doping concentration in doped 4H-SiC epilayers by low temperature photoluminescence, Phys. Scripta 72 (2–3) (2005) 254–257.
[93] I. Ivanov, et al., Nitrogen doping concentration as determined by photoluminescence in 4H- and 6H-SiC, J. Appl. Phys. 80 (1996) 3504–3508.
[94] S. Asada, T. Kimoto, I.G. Ivanov, Calibration on wide-ranging aluminum doping concentrations by photoluminescence in high-quality uncompensated P-type 4H-SiC, Appl. Phys. Lett. 111 (2017): 072101.
[95] S. Juillaguet, et al., Dilute aluminium concentration in 4H-SiC: from SIMS to LTPL measurements, Mater. Sci. Forum 457–460 (2004) 775–778.
[96] E.R. Glaser, et al., Infrared PL signatures of n-type bulk SiC substrates with nitrogen impurity concentration between 10^{16} and 10^{17} cm^{-3}, Mater. Sci. Forum 600–603 (2009) 449–452.
[97] M. Odawara, et al., Defects grouping and characterizations of PL-imaging methods for 4H-SiC epitaxial layers, Mater. Sci. Forum 778–780 (2014) 382–385.
[98] P. Berwian, et al., Imaging defect luminescence of 4H-SiC by ultraviolet-photoluminescence, Solid State Phenom. 242 (2016) 484–489.
[99] F. Oehlschläger, et al., Photoluminescence-topography of the P-type doped SiC wafers for determination of doping inhomogeneity, Mater. Sci. Forum 615–617 (2009) 259–262.
[100] B. Krishnan, S.K. Chanda, Y. Koshka, Properties of different room-temperature photoluminescence bands in 4H-SiC substrates investigated by mapping techniques, Mater. Sci. Forum 556–557 (2007) 411–414.
[101] S. Chanda, Y. Koshka, M. Yoganathan, Relationship between infrared photoluminescence and resistivity in semi-insulating 6H-SiC, J. Electron. Mater. 35 (2006) 630–634.